Local-density-derived semiempirical nonlocal pseudopotentials for InP with applications to large quantum dots

Huaxiang Fu and Alex Zunger
National Renewable Energy Laboratory, Golden, Colorado 80401
~Received 5 August 1996!

In the same way that *atomic* calculations have been used previously to extract *bare* ionic pseudopotentials, self-consistent *bulk* calculations can be used to construct *screened* atomic pseudopotentials. We use such a method to construct screened nonlocal atomic pseudopotentials for InP. A series of bulk, local-density-approximation ~LDA! calculations are performed on a few InP crystal structures, covering a range of unit-cell volumes, to produce bulk potentials V_{LDA}~**G**!‰. By solving a set of linear equations, we extract from these crystalline potentials the corresponding screened *atomic* ''spherical LDA'' ~SLDA! potentials *v*

such that the wave functions are LDA-like while the band structures, effective masses, and deformation potentials match experiments. Here we apply this ''semiempirical pseudopotential method'' ~SEPM! to both the bulk structure and nanostructures of InP.

The present work differs from our previous work[13] in several aspects:

~i! We develop and apply pseudopotentials for a new material system—bulk InP and InP quantum dots on which numerous experiments have been recently performed,[18–23] but little theoretical work is available. InP dots have been recently synthesized either as strain-induced ''self-assembled'' particles in metalorganic vapor phase epitaxy,[20,21] or as particles in colloidal solution growth.[22,23] The dot sizes range from 20 to 600 Å. Some interesting phenomena were found, e.g., the evolution of photoluminescence ~PL! intensity with pressure,[18] the strong dependence of PL decay time on the photon energy,[19] the blueshift of the PL peak with the photoexcitation power, and band-gap renormalization effects.[20,21] Quantitative analyses of such experiments require a practical and reliable computational tool, which can reproduce excitation energies, wave-function information ~e.g., transition probabilities!, effective masses, and deformation potentials. The present method is suitable for such purposes.

~ii! We wish to understand the limitation of the SEPM. The SEPM approach[13] relies on representing the screened solid-state pseudopotential as linear combination of overlapping but *spherical* ''site potentials,'' and on system-to-system transferability. If such potentials are transferable from one structure to another, their Fourier transforms will lie on a ''universal'' potential-versus-momentum curve. We have seen previously[13] that both the spherical approximation and the transferability approximation work very well for Si and CdSe. But unlike Si and CdSe, the atomic size difference between In and P is very large, so the directional charge transfer in InP could be significant, raising questions on the suitability of the spherical approximation. Indeed, we find that there is a larger error for InP in the b-Sn structure than in the zinc-blende and rocksalt structures. We further find that the asymmetric part of the InP ''spherical LDA'' ~SLDA!

$$V_{\mathrm{LDA}}^{s}(\mathbf{G}) = \sum_{a} S^{a,s}(\mathbf{G})\, v_{\mathrm{SLDA}}^{a,s}(|\mathbf{G}|), \qquad (3)$$

where $S^{(a,s)}(\mathbf{G}) = \frac{1}{N_s} \sum_{\mathbf{R}_{a,s}} e^{i\mathbf{G}\cdot\mathbf{R}_{a,s}}$ is the structure factor and $\mathbf{G}$ is a reciprocal lattice vector. Note that $v_{\mathrm{SLDA}}^{a,s}$ is not a free-atom potential, but rather a solid-embedded site potential. The SLDA site potentials can be written conveniently as a symmetric part $v_{\mathrm{SLDA}}^{1}(|\mathbf{G}|)$ and an asymmetric part $v_{\mathrm{SLDA}}^{2}(|\mathbf{G}|)$:

$$v_{\mathrm{SLDA}}^{1}(|\mathbf{G}|) = v_{\mathrm{SLDA}}^{\mathrm{In}}(|\mathbf{G}|)$$

ued at the shortest bulk **G** vectors. This deviation of $v^{(2)}_{\mathrm{SLDA}}$ 3(|**G**|) from a universal curve did not occur in Si @for which $v^{\tilde{}2!}_{\mathrm{SLDA}}$~|**G**|! [0# or in CdSe ~see Fig. 1 in Ref. 13!. We also observe that this nontransferability error is mainly reflected in the asymmetric potential $v^{\tilde{}2!}_{\mathrm{SLDA}}$~|**G**|!, while the symmetric potentials *v*

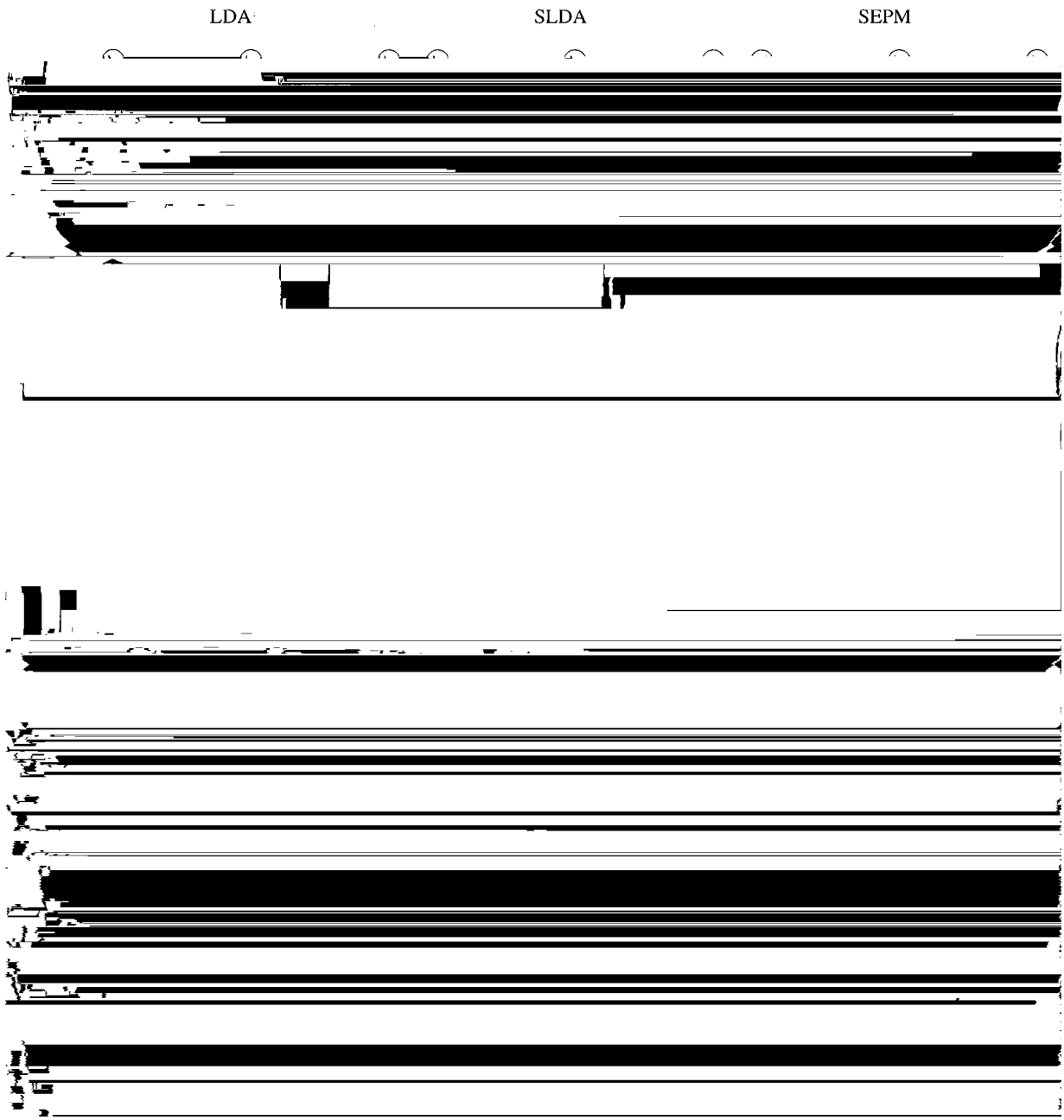

FIG. 3. Contour plots of wave-function squares on the ~110! plane for the Γ_{15v}, Γ_{1c}, X_{5v}, and X_{1c} states in zinc-blende InP ~lattice constant a 5 11.01 a.u.! as calculated by using LDA, SLDA, and SEPM potentials. The LDA and SLDA results are obtained using kinetic cutoff energy $E_{\rm cut}$ 5 25 Ry, and the SEPM results are obtained using $E_{\rm cut}$ 5 6.8 Ry and the Gaussian correction ~Appendix B!.

averaged errors between the LDA and the SLDA results are 0.07 and 0.02 eV for the lowest eight bands in zinc-blende and rocksalt InP, respectively. In the metallic β-Sn form, the error is larger: 0.35 eV for the first and fifth bands and 0.1 eV for other bands. In order to find the reason for this relatively large error, we intentionally let the fitted curve in Fig. 1~b! pass through the β-Sn data points. Application of this potential to study the band structure will result in error reflecting only the spherical approximation. We find that in the β-Sn structure the spherical approximation error is about 0.15 eV and the nontransferability error is 0.20 eV for the first and fifth bands. We attribute the relatively larger error for β-Sn structure to the large difference in the sizes of the In and P atoms, and to the low symmetry of the β-Sn structure.

We find that the LDA wave functions are also accurately reproduced by our fitted SLDA potentials. As an example, Fig. 3 compares the contour plots of the wave-function squares for the Γ_{15v}, Γ_{1c}, X_{5v}, and X_{1c} states of zinc-blende InP as calculated from the LDA and from the fitted SLDA potentials. The agreement is excellent: the LDA versus SLDA wave-function overlap is larger than 99.9%.

The first three columns in Table I[29–41] compare zinc-blende InP band energies, effective masses, and deformation potentials obtained from LDA and SLDA calculations, showing good agreement.

The good agreement between LDA and SLDA calculations persists after we reduce the kinetic cutoff energy from 25 to 6.8 Ry, while compensating for the reduced basis by

using the ''Gaussian correction'' ~GC! method[13] as described in Appendix B and in Fig. 4. The reduction of the kinetic energy cut-off can reduce significantly the computational effort for quantum nanostructures.

B. SEPM potentials and their performance for bulk InP

In the next step, we apply linear changes to the curve-fitted potentials $v_{\mathrm{SLDA}}^{\sim 6!}(|\mathbf{G}|)$ @i.e., we only change the coefficients $\{c_i\}$ in Eq. ~6!# so as to fit their bulk eigenvalues to the experimentally observed excitations. The obtained potential is called the SEPM potential. The required changes in the potentials are found to be small, and therefore the changes in the wave functions relative to the LDA calculation are also small.

Table I compares the band energies, effective masses, and deformation potentials obtained by using the SLDA potential and the empirically corrected potential ~SEPM!. In this table, the pertinent experimental results are included for comparison. We see that the SEPM achieves good accord with the pertinent experimental quantities, including the band structures at Γ, X, and L points, the effective masses and deformation potentials. The SEPM band structures of InP in zinc-blende structures are compared in Fig. 5 with the SLDA band structures. We see that, except for the upshifts of the conduction bands, the main features and trends of the whole

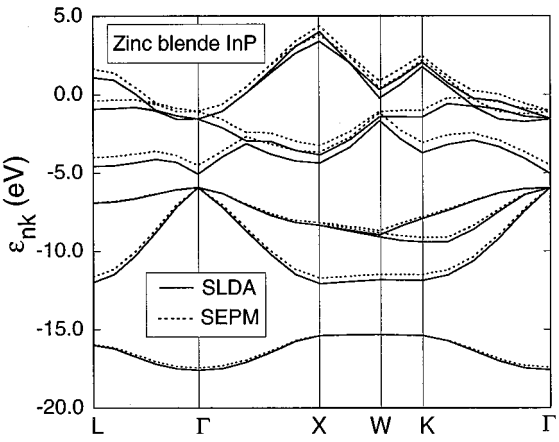

FIG. 5. The zinc-blende InP band structure calculated from SEPM ~dotted lines! and from SLDA potentials ~solid lines!. The lattice constant is $a = 11.01$ a.u. Both the SEPM and the SLDA band energies are given in absolute values. Since the VBM positions are very close to each other for LDA and SLDA bands, this figure shows that most of the LDA error is in the conduction bands.

formed from the *s* orbitals of the two atoms! is mainly determined by the atomic energy level of the In *s* orbital. The increase of the SEPM potential relative to the SLDA potential in the In core region will push up the atomic energy level

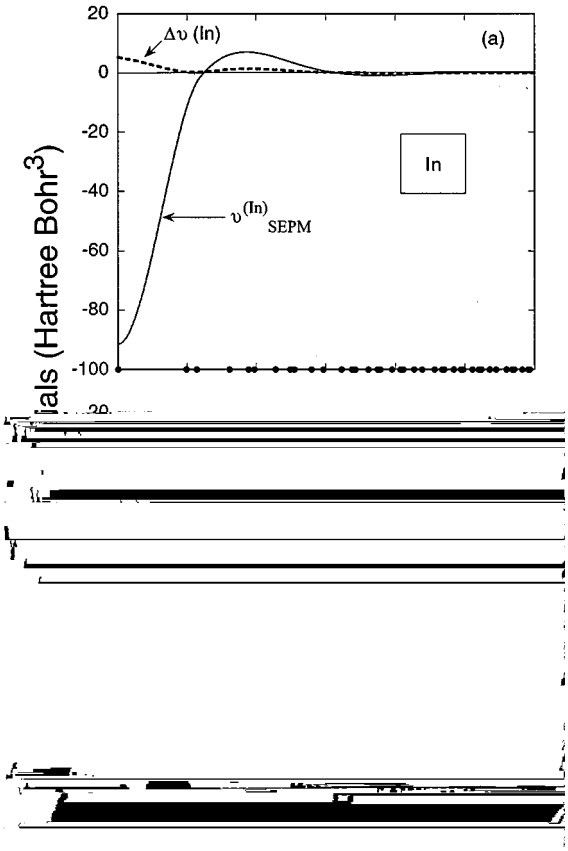

FIG. 6. The semiempirical atomic potentials $v^{a!}_{SEPM}$ ~solid lines! and the shift $\Delta v = v^{a!}_{SEPM} - v^{a!}_{SEPM}$ ~dotted lines! in **G** space: ~a! for In; ~b! for P. Dots on the axis indicate zinc-blende reciprocal-lattice-vector lengths for bulk InP.

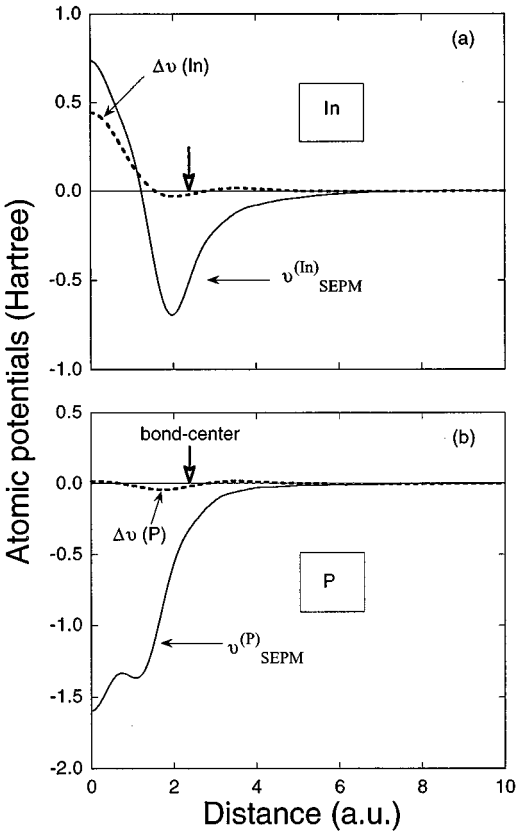

FIG. 7. The semiempirical atomic potentials $v^{a!}_{SEPM}$ ~in solid lines! and the shift Δ

of the In *s* orbital, consequently raising the lowest conduction band. Due to the orthogonalization constraint, the higher conduction bands will also be pushed up as shown in Fig. 5. The valence bands bear only little change since the *p* orbital energy is not affected by shifting the In potential near the origin. Furthermore, since the potentials near the In-P bond center do not change significantly, the In-P interaction will not change much. This suggests that the wave function will not change too much either. This is borne out by the similarity of SEPM and LDA wave functions shown in Fig. 3. The fact that the error in SLDA potential is mostly in the atomic core region and is different for *s* and *p* valence electrons suggests that one could improve the SEPM fit by treating the nonlocal part of the pseudopotential also as a parametrized function. At this stage, however, we prefer not to introduce additional fitting functions.

(ii) Energy location of the LDA error: Figure 5 gives the SEPM and SLDA bands of zinc-blende InP *on an absolute scale* ~i.e., the VBM's are not aligned!. The comparison of SEPM band structures relative to SLDA results shows that the main effect of the removal of LDA error is to move the conduction bands up while the valence bands do not change much. This situation is similar to what was found in more elaborated *GW* calculations.[42]

D. Effect of the potential slope at G = 0 on nanostructures

So far, our discussion has centered on bulk materials. Application of SEPM potentials to quantum nanostructures

~which contain reciprocal lattice vectors that are absent in the bulk! requires that the potentials should be flat near $\mathbf{G}=0$ i.e., the potential slope at $\mathbf{G}=0$ is zero. As an illustration of this point, we calculated the planar-averaged potential $\bar{V}_a(z)$ for ~110!-oriented InP films with different thicknesses, using the SEPM potentials ~i! with nonzero slope and ~ii! with zero slope at $\mathbf{G}=0$. Here,

$$\bar{\bar{V}}_a(z) = \frac{1}{2l}\int_{z-l}^{z+l} \overline{V}(z')\,dz', \tag{7}$$

where

$$\overline{V}(z) = \frac{1}{S}\int V(\mathbf{r})\,dx\,dy, \tag{8}$$

$$V(\mathbf{r}) = \sum_{a}\sum_{\mathbf{R}_i} v^{a}_{\mathrm{SEPM}}(\mathbf{r}-\mathbf{R}_i). \tag{9}$$

In the above equations, z is the distance from one side of the supercell along the direction vertical to the film, and S is the area of cross section parallel to the film plane. l is the thickness of a single monolayer in the InP~110! film. The planar-averaged potential $\bar{\bar{V}}_a(z)$ for films with different thicknesses are shown in Fig. 8~a! for the SEPM potentials with nonzero slope, and in Fig. 8~b! for the SEPM potentials with zero slope at $\mathbf{G}=0$. It can be seen that in Fig. 8~a! the potential at the slab center has not approached the bulk value even for 15-ML-thick films while the potential in Fig. 8~b! has achieved the bulk value at the film center even for rather thin films. This $\mathbf{G}=0$ treatment has no effect on the properties of bulk InP, but is crucial for the investigation of quantum confinement effect in nanostructures such as in dots. The slopes of the SEPM potentials generated previously[13] for Si and CdSe are very close to zero too.

The final InP SEPM as well as the Si and CdSe potentials can be found on an FTP site for the interested readers.[43] They can be used in numerous applications requiring large-scale calculations.

IV. APPLICATIONS TO QUANTUM DOTS

As an illustration of the utility of our semiempirical pseudopotential, we use it to calculate the band gaps of surface-passivated InP quantum dots with different sizes. Here we discuss only the salient features of the results. A detailed description of InP quantum dot will be deferred to a future paper.

We consider InP dots containing 17, 29, 107, 259, and 712 atoms ~not including the passivating atoms!. The dots take cubic shape with faces oriented along the ~001! and ~110! planes of zinc-blende structure. Using the same density as in the bulk, the effective dot sizes are calculated by $D=(a/2)(N)^{1/3}$ where a is the lattice constant and N is the number of atoms in the dots. This gives effective sizes $D=7.49$, 8.95, 13.83, 18.57, and 26.01 Å for the dots with 17, 29, 107, 259, and 712 atoms, respectively.

We next discuss the surfaces of the dots. Previous calculations on other-material dots using the $\mathbf{k}\cdot\mathbf{p}$ theory,[44] tight-binding method,[45] or truncated crystal method[46] have ignored the existence of surfaces either by assuming infinite potential barrier or by removing the dangling bonds in the Hamiltonian matrix. Since one of our future objectives is to

include here explicit surface effects. For bare

lar to the z axis, respectively. For the InP dots considered here, the x, y, and z axes are along ~110!, ~110!, and ~001! directions of InP zinc-blende structure, respectively. The x and y directions are equivalent for the dots considered here. Figures 10~a! and 10~b! give, respectively, the planar-averaged wave-function squares $\overline{|c_m|^2}(x)$ and $\overline{|c_m|^2}(z)$ for the dot with 712 atoms. In this figure, symbols along the horizontal axis indicate atomic-layer positions in the dot. From Fig. 10, we can see that the wave functions of both the CBM and VBM are mostly distributed in the interior of dot, with but little amplitude at the dot surface. For such ''dot-interior'' states, changes in the passivation potential ~e.g., different saturation species! cannot shift these energy levels significantly. A similar situation is found in experiments.[22,23]

In summary, we derive the semiempirical pseudopotentials for InP from *ab initio* LDA pseudopotential calculations. The obtained SEPM potentials reproduce accurately the LDA wave functions and the experimentally observed band structures, effective mass, and deformation potential. Since it is soft, the SEPM potential can be used efficiently in large-scale quantum nanostructure calculations using plane-wave bases. This is illustrated here for the band gaps of InP

$v_{\mathrm{SLDA}}^{\tilde{}1!}{}^{\sim}r!5@a_1$

[28] D. R. Hamann, M. Schluter, and C. Chiang, Phys. Rev. Lett. **43**, 1494 ~1979!.
[29] J. van Laar, A. Huijser, and T. L. van Rooy, J. Vac. Sci. Technol. **14**, 894 ~1977!.
[30] L. Ley and R. A. Pollak, Phys. Rev. B **9**, 600 ~1974!.
[31] Z. Hang, H. Shen, and F. H. Pollak, Solid State Commun. **36**, 15 ~1990!.
[32] P. Lautenschlager, M. Garriga, and M. Cardona, Phys. Rev. B **36**, 4813 ~1987!.
[33] S. W. Tozer, D. J. Wolford, J. A. Bradley, D. Bour, and G. B. Stringfellow, *Proceedings of the 19th ICPS, Warsaw, Poland*, edited by W. Zawadski ~Institute of Physics, Polish Academy of Sciences, 1988!, p. 881.
[34] L. W. James, J. P. Van Dyke, F. Herman, and D. M. Chang, Phys. Rev. B **1**, 3988 ~1970!.
[35] P. Rochon and E. Fortin, Phys. Rev. B **12**, 5803 ~1975!.
[36] J. M. Chamberlain, J. Phys. C **4**, L38 ~1971!.
[37] J. Leotin, R. Barbaste, S. Askenazy, M. S. Skolnick, R. A. Stradling, and J. Tuchendler, Solid State Commun. **15**, 693 ~1974!.